European Journal of Pharmacology 1003 (2025) 177932

Contents lists available at ScienceDirect

European Journal of Pharmacology

journal homepage: www.elsevier.com/locate/ejphar

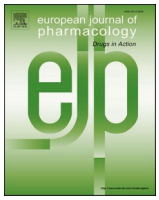

Investigation of the effects of losartan and captopril on rotenone-induced inflammation via TLR4/NLRP3 pathway: An integrative *in vitro* and *in silico* study

Dilara Nemutlu Samur

Alanya Alaaddin Keykubat University, Faculty of Medicine, Department of Pharmacology, 07450, Antalya, Turkey

ARTICLE INFO

Keywords:
Parkinson's disease
Inflammation
TLR4
NLRP3
Losartan
Captopril
Rotenone

ABSTRACT

Neuroinflammation is a key contributor to neurodegenerative diseases, including Parkinson's disease (PD). Non-motor symptoms such as gut-derived inflammation often precede motor deficits and represent an early stage of PD pathology. We aimed to investigate the anti-inflammatory potential of losartan and captopril on rotenone-induced inflammation in enteric glial cells (EGCs), focusing on the modulation of the TLR4/NLRP3 inflammasome signaling pathway. EGCs were treated with rotenone (1 μM) to induce inflammation. Non-cytotoxic drug concentrations (10–100 μM) were identified by cell viability assays. Caspase-1 and IL-1beta levels were quantified via ELISA, and mRNA expression of TLR4/NLRP3 was assessed by RT-qPCR. Molecular docking was performed to predict drug interactions with TLR4 and NLRP3 proteins. Rotenone significantly increased caspase-1 levels and TLR4/NLRP3 expression. Losartan at 10 μM significantly reduced rotenone-induced NLRP3 mRNA expression, while captopril required a higher concentration (100 μM) for a comparable inhibitory effect. Paradoxically, losartan and captopril alone increased caspase-1 and/or TLR4 expression, suggesting dose-dependent pro-inflammatory effects. Molecular docking showed a stronger binding affinity for losartan compared to captopril toward TLR4/NLRP3 proteins, consistent with observed biochemical effects. Our results highlight the therapeutic potential of losartan and captopril as modulators of TLR4/NLRP3-mediated inflammation.

1. Introduction

Neuroinflammation is a key mechanism of neurodegenerative diseases (Suleiman Khoury et al., 2024). Among them, Parkinson's disease (PD) stands out due to its well-documented link with peripheral inflammatory events, particularly those originating within the gut-brain axis (Bonaz, 2024). Inflammation in the intestine appears particularly relevant in the development of non-motor manifestations of PD that may precede motor symptoms by decades (Houser and Tansey, 2017). Recent epidemiological studies indicate that chronic intestinal inflammatory conditions like inflammatory bowel disease are associated with a higher risk of developing PD (Brudek, 2019), supporting the concept that intestinal inflammation can contribute to PD pathogenesis. Additionally, gastrointestinal barrier dysfunction and inflammation may trigger systemic inflammation that promotes neurodegeneration via the vagus nerve and immune pathways (Zeng et al., 2022). Studies shows that gut inflammation may induce the loss of dopaminergic neurons, a hallmark of PD (Garrido-Gil et al., 2018; Villarán et al., 2010). Chronic inflammation is driven by complex molecular pathways involving various pattern recognition receptors including Toll-like receptors (TLRs) (Kielian, 2006). Among these receptors, TLR4 is especially of interest for its ability to sense damage-associated molecular patterns (DAMPs) and initiate inflammatory pathways that contribute to neurodegenerative processes. Upon activation, TLR4 initiates downstream signaling, which leads to the activation of the nucleotide-binding oligomerization domain (NOD)-like receptor pyrin domain-containing 3 (NLRP3) inflammasome, a critical mediator of triggering pro-inflammatory cytokines such as interleukin-1β (IL-1β) and caspase-1, thus promoting the neuroinflammatory response (Zhang and Yang, 2023). Recent data propose that dysbiosis increases intestinal permeability and abnormally stimulates TLR4/TLR2 signaling in the gut, creating an inflammatory condition that promotes α-synuclein misfolding in enteric neurons. These aggregates propogate via the vagus nerve to the brain, triggering TLR/NLRP3-mediated neuroinflammation and accelerating neurodegeneration (Gorecki et al., 2021).

Rotenone, a commonly used inhibitor of mitochondrial complex I, has been utilized in research models to replicate PD-like pathology because of its capacity to trigger oxidative stress, mitochondrial

E-mail address: dilara.samur@alanya.edu.tr.

https://doi.org/10.1016/j.ejphar.2025.177932
Received 18 March 2025; Received in revised form 7 July 2025; Accepted 8 July 2025
Available online 9 July 2025

impairment, and neuroinflammation (Umer et al., 2025). Rotenone-induced neurotoxicity has been shown to activate TLR4 and NLRP3 pathways, making it an ideal agent for investigating potential anti-inflammatory therapies targeting these signaling mechanisms (Perez-Pardo et al., 2018; Won et al., 2015). Enteric glial cells (EGCs), the gut-resident counterparts of brain astrocytes, are increasingly valued for their central role in intestinal inflammation control and neural integrity (Cirillo et al., 2011). EGCs actively regulate immune responses, survival of neurons, and gut-brain communication (Santhosh et al., 2024). Given that gastrointestinal disturbances and gut-derived inflammatory signals are among the earliest manifestations of PD (Montanari et al., 2023), investigating neuroinflammatory pathways in EGCs provides a physiologically relevant approach to understand disease mechanisms and therapeutic targets.

Considering the clinical significance of TLR4 and NLRP3 in neuroinflammatory disorders, the pharmacological modulation of these pathways offers a hopeful therapeutic strategy. The brain renin-angiotensin system (RAS) plays a significant role beyond its traditional role in blood pressure and contributes to neuroinflammation, oxidative stress, and neurodegeneration (Labandeira-Garcia et al., 2024). Angiotensin II, one of the most critical components of the system, induces inflammation by inducing microglial activation and increasing pro-inflammatory cytokine expression via the TLR4 and NLRP3 inflammasome pathways. (Espitia-Corredor et al., 2022; Tamura et al., 2015). Losartan, an angiotensin II receptor antagonist, and captopril, an angiotensin-converting enzyme (ACE) inhibitor, are commonly used in cardiovascular diseases and have demonstrated anti-inflammatory properties beyond their classical roles in blood pressure regulation (Sepehri et al., 2016). In this study, we aimed to evaluate the inhibitory effects of losartan and captopril on rotenone-induced inflammation in EGCs, specifically focusing on the modulation of the TLR4/NLRP3 signaling pathway. By elucidating these mechanisms, our findings may contribute to therapeutic strategies targeting early neuroinflammatory events in PD.

2. Materials and methods

2.1. In vitro studies

2.1.1. Chemicals and reagents

Rotenone, losartan, and captopril were obtained from Sigma-Aldrich (St. Louis, MO, USA). Culture media and supplements were purchased from Gibco (New York, USA). ELISA kits for detecting IL-1β and caspase-1 were obtained from BT Lab (Zhejiang, China).

2.1.2. Enteroglial cell culture

The rat enteroglial cell line was generously provided by Dr. Luca Antonioli (University of Pisa). The cells were maintained in DMEM supplemented with 10 % fetal bovine serum (FBS), 2 mM L-glutamine, and 100 U/mL penicillin-streptomycin. Cells were incubated at 37 °C in a humidified atmosphere with 5 % CO2. Upon reaching 70–80 % confluency, cells were detached using trypsin-EDTA and seeded into T-25 flasks and 96-well plates for further analysis.

2.1.3. MTT assay for cell viability

Cell viability was evaluated using the MTT (3-(4,5-dimethylthiazol-2-yl)-2,5-diphenyl-2H-tetrazolium bromide) assay, following the procedure described by (Grela et al., 2018). Briefly, following 24-h treatments with losartan (100 nM–1000 μM) or captopril (100 nM–1000 μM), the culture medium was removed, and cells were resuspended in phosphate-buffered saline (PBS; 0.01 M, pH 7.4). MTT solution (5 mg/mL in PBS) was added to each well of the 96-well plate containing treated cells. The plates were incubated for 4 h at 37 °C. After incubation, the supernatant was carefully removed, and 100 μL of dimethyl sulfoxide (DMSO) was added to each well to dissolve the formazan crystals formed by metabolically active cells. The absorbance was measured at 570 nm using a microplate reader (Synergy H1, Biotek, USA). Cell viability was calculated as a percentage relative to the untreated control group (considered 100 % viability).

2.1.4. Reverse transcription quantitative polymerase chain reaction (RT-qPCR)

Total RNA was extracted from cells using the RNA Isolation Kit (HibriGen, Cat. No. MG-RNA-01-100) following the manufacturer's protocol. Briefly, cells were lysed, and total RNA was isolated using spin-column purification. RNA quality and concentration were assessed spectrophotometrically, and samples with an OD 260/280 ratio between 1.7 and 2.0 were used for further analysis. For cDNA synthesis, 1 μg of total RNA was reverse transcribed using the OneScript® Plus cDNA synthesis kit (ABM, G236). The reaction mixture included 4 μL of RT buffer, 1 μL each of reverse transcriptase, dNTP mix, oligo-dT primers, and random primers in a total volume of 20 μL. The mixture was incubated at 25 °C for 10 min, 50 °C for 15 min, and then heated to 85 °C for 5 min to terminate the reaction. The synthesized cDNA was stored at −80 °C until use.

The sequence for the primer sets used for the target genes (TLR4 and NLRP3) are shown in Table 1. PCR amplification was performed using a Roche LightCycler 96 system. The reaction conditions were as follows: pre-denaturation at 95 °C for 5 min, followed by 40 cycles of denaturation at 95 °C for 15 s and annealing/extension at 60 °C for 20 s. A melting curve analysis was performed from 60 °C to 95 °C, with a 0.5 °C increase per second, to verify the specificity of the PCR products. The relative fold-change quantification of each gene was calculated by the $2^{-\Delta\Delta CT}$ method (Schmittgen and Livak, 2008) using the reference gene beta-actin (β-act) for normalization.

2.1.5. Enzyme-linked immunosorbent assay

The levels of inflammatory cytokines, caspase-1 and IL-1β were quantified in EGCs lysates using enzyme-linked immunosorbent assay (ELISA) kits. Commercially available ELISA kits for rat caspase-1 (BT Lab, E1897Ra) and IL-1β (BT Lab, E0119Ra) were used according to the manufacturer's instructions. Briefly, cells were washed with PBS, gently trypsinized, and collected into centrifuge tubes. The suspension was centrifuged at 1000 g for 5 min, and the supernatant was discarded. Cells were washed with PBS three times to remove any residual media. Each 1 × 106 cells were resuspended in 150–250 μL of PBS, and the cells were subjected to three freeze-thaw cycles to ensure complete lysis. The lysates were then centrifuged at 1500 g for 10 min at 2–8 °C, and the supernatant was collected for ELISA analysis. The supernatants were stored at −20 °C until further use. All measurements were performed in triplicate.

2.2. Molecular docking analysis

2.2.1. Protein preparation

The three-dimensional (3D) structures of TLR4 (PDB ID: 3FXI) and NLRP3 (PDB ID: 6NPY) were downloaded from the Protein Data Bank (PDB). Using ChimeraX v1.9, unnecessary water molecules and non-essential ligands were removed prior to docking and loaded to SwissDock in an appropriate format. SwissDock employs a blind docking strategy using the AutoDock Vina algorithm, which automatically scans the entire protein surface to predict the most favorable binding pockets based on energy calculations. Therefore, no predefined binding region

Table 1
Primer sequences used for RT-qPCR analyses.

Gene	Primer Sequence
TLR4	F: GGATGATGCCTCTCTTGCAT R: TGATCCATGCATTGGTAGGTAA
NLRP3	F: GTGGAGATCCTAGGTTTCTCTG R: CAGGATCTCATTCTCTTGGATC

was specified. The binding sites and clusters generated by SwissDock represent the lowest-energy binding conformations across the entire protein surface.

2.2.2. Ligand preparation

The canonical SMILES of losartan (PubChem CID: 3961) and captopril (PubChem CID: 44093) were obtained from the PubChem (https://pubchem.ncbi.nlm.nih.gov/) (accessed on September 12, 2024) and uploaded to the SwissDock platform.

2.2.3. Docking protocol

The *Autodock Vina* algorithm provided by SwissDock was used for evaluating the binding affinities of ligands. A grid box was generated around the active sites of TLR4 and NLRP3 based on previous studies identifying key residues involved in ligand binding. For each docking run, the grid box dimensions were set to 30 × 30 × 30 Å to encompass the predicted binding pocket. The center of the grid was adjusted for each target protein depending on the predicted ligand-binding region (Box center: 107.0, 103.0, 101.0 for NLRP3 and Box center: 16.0 1.0 7.0 for TLR4). The spacing between grid points used was the default value (0.375 Å) and the sampling exhaustivity was set to 20 to ensure reliable pose prediction. All other parameters were kept at default values provided by the SwissDock platform. To validate and contextualize our molecular docking results, we included TAK-242 and MCC950 as positive control compounds for TLR4 (Matsunaga et al., 2011) and NLRP3 (Coll et al., 2019), respectively. The binding affinities (kcal/mol) and binding poses were analyzed to identify the most favorable interactions between the ligands and the proteins.

2.2.4. Visualization of results

Output files and three-dimensional binding positions provided by SwissDock were visualized using ChimeraX v1.9 for detailed structural analysis. The binding affinities of losartan and captopril to TLR4 and NLRP3 were assessed using results from docking studies, which allowed for an evaluation of their potential interactions. To enhance the visualization of bindings, we included supplementary spin videos demonstrating the three-dimensional docking conformation and key interactions (Supplementary Videos 1-4).

2.3. Statistical analysis

Data were expressed as the mean ± standard error of mean (SEM). Before performing parametric tests, data distributions were tested for normality using the Kolmogorov–Smirnov test. Differences between groups in behavioral tests were analyzed using one-way ANOVA followed by Tukey post-hoc test. For the data sets which did not follow the normal distribution, the Kruskal-Wallis test was performed followed by Dunn's test for post-hoc comparison between groups. All statistical analyses were performed using GraphPad Prism 10.0 software (SanDiego, CA, USA). A P-value less than 0.05 was considered statistically significant.

3. Results

3.1. Cell proliferation analysis (MTT assay)

The 24-h treatment with losartan led to a significant reduction in cell proliferation at concentrations of 1000, 500, and 250 μM, with decreases of 93.62 %, 89.07 %, 90.63 %, respectively, compared to the control group (Fig. 1a). At concentrations below 250 μM, losartan did not exhibit any cytotoxic effects on the cells. Based on these findings and relevant literature data, the concentration of 100 μM was selected for subsequent experiments.

The 24-h treatment with captopril led to a significant reduction in cell proliferation at concentrations of 500 and 250 μM, with decreases of 22.33 % and 22.39 %, respectively, compared to the control group (Fig. 1b). 1000 μM concentration paradoxically increased the cell proliferation significantly (12.71 %) compared to the control group. At concentrations below 250 μM, captopril did not exhibit any cytotoxic effects on the cells. Based on these findings and relevant literature data, the concentration of 100 μM was selected for subsequent experiments.

In our previous work using EGCs, JC-1 assay (mitochondrial membrane potential) results led us to select 10 μM as the working concentration for rotenone (Samur et al., 2025). However, further investigations revealed that 10 μM of rotenone strongly suppressed immune responses, disrupting inflammatory signaling pathways. This aligns with recent findings indicating that rotenone may exert immunosuppressive effects on glial cells (Rabaneda-Lombarte et al., 2019, 2020). Therefore, to prevent unintended immunosuppression while maintaining an appropriate inflammatory response, 1 μM was selected as the optimal concentration for rotenone in this study.

3.2. Changes in caspase-1 and IL-1β levels in enteric glial cells

The levels of caspase-1 and IL-1β were analyzed in EGCs to evaluate differences between the groups (Fig. 2a). When comparing caspase-1

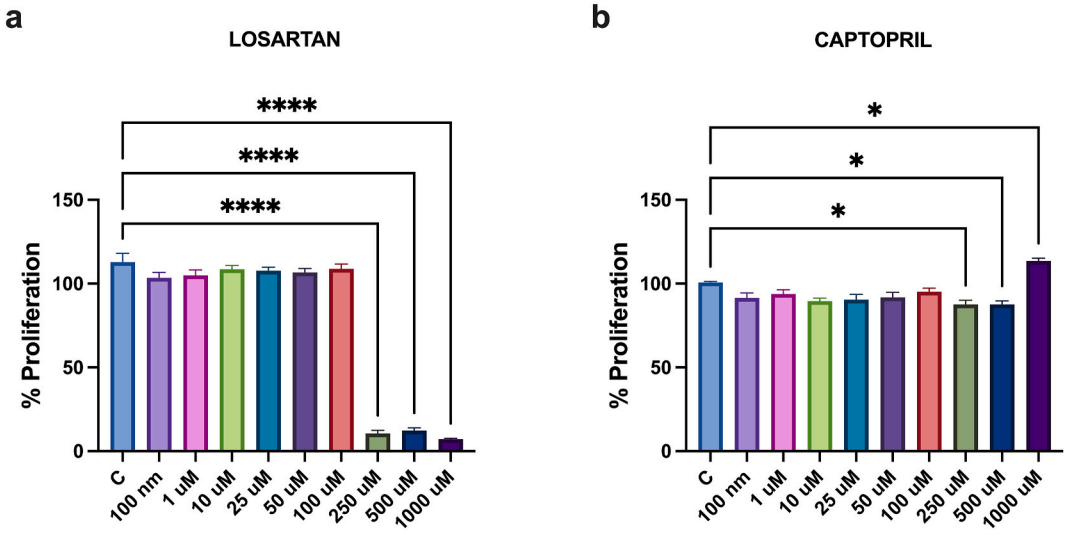

Fig. 1. The effects of losartan (a) and captopril (b) on cell proliferation. Comparison of percentage proliferation values across different concentrations. Data were obtained from experiments performed in eight replicates and repeated three times. *$p < 0.05$, ****$p < 0.0001$.

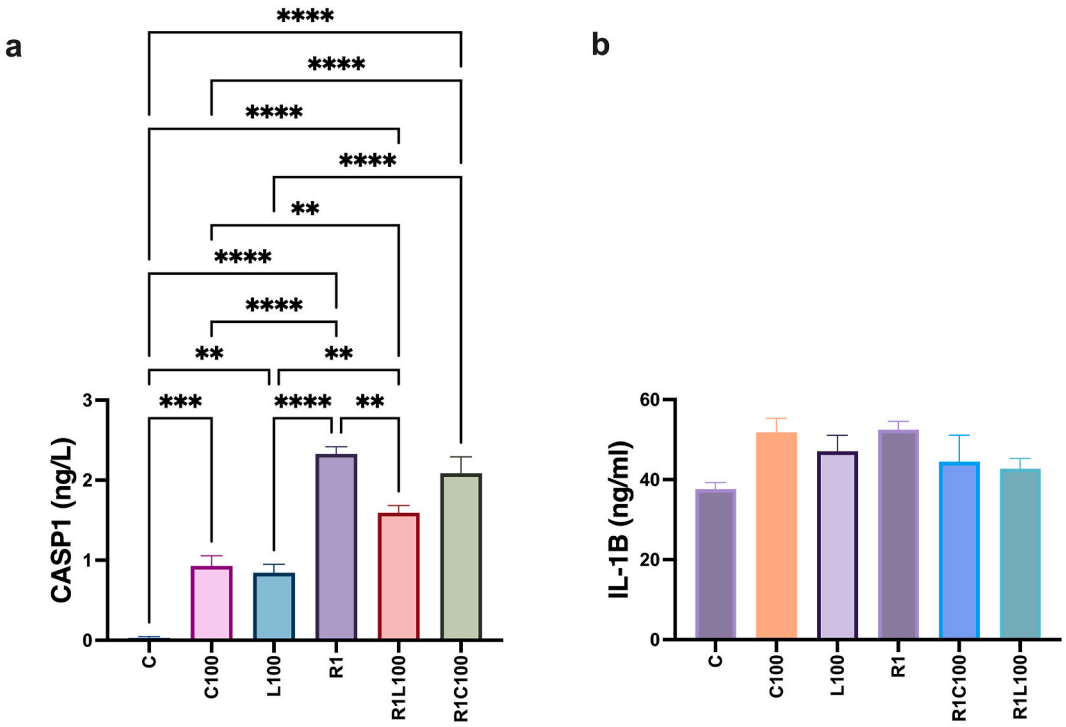

Fig. 2. Changes in caspase-1 (CASP1) (a) and IL-1beta (IL-1β) (b) levels in enteric glial cells. Data are expressed as mean ± SEM. Statistical significance was determined by one-way ANOVA followed by Tukey's post hoc test. *$p < 0.05$, **$p < 0.01$, ***$p < 0.001$, ***$p < 0.0001$. C: Control, R1: 1 μM Rotenone, C100: 100 μM captopril, L100: 100 μM losartan.

levels across the experimental groups, statistically significant differences were observed (One-way ANOVA: F (5, 16) = 52.37, $P < 0.0001$). Post-hoc analysis using Tukey's multiple comparisons test revealed that caspase-1 levels were significantly increased in the rotenone-treated group compared to the control group ($P < 0.001$). Losartan administration with rotenone (ROT + L100), significantly decreased caspase-1 levels compared to the rotenone group ($P < 0.01$). Although captopril administration resulted in a 10.39 % decrease in caspase-1 levels compared to the rotenone group, this reduction was not statistically significant. Interestingly, captopril and losartan caused a significant increase in caspase-1 levels compared to the control group ($P < 0.01$ and $P < 0.001$, respectively). However, this increase was significantly lower than the rotenone group ($P < 0.0001$ for both).

One-way ANOVA analysis showed no statistically significant differences in IL-1β levels among the treatment groups (F (5, 15) = 1.896, P = 0.1549), indicating that neither rotenone nor its combination with captopril and losartan led to a significant modulation of IL-1β expression (Fig. 2b).

3.3. Changes in TLR4 and NLRP3 mRNA expression in enteric glial cells

The mRNA levels of TLR4 and NLRP3 were analyzed in EGCs to evaluate differences between the groups (Fig. 3). When comparing TLR4 and NLRP3 mRNA expression across the experimental groups, statistically significant differences were observed (for losartan-treated groups, One-way ANOVA: F (5, 12) = 39.71, $P < 0.0001$ for TLR4 and F (5, 13) = 15.70, $P < 0.0001$ for NLRP3; for captopril-treated groups, One-way ANOVA: F (5, 12) = 47.28, $P < 0.0001$ for TLR4 and F (5, 12) = 14.70, $P < 0.0001$ for NLRP3). Post-hoc analysis using Tukey's multiple comparisons test revealed that 100 μM losartan (L100) led to an extreme upregulation of TLR4 and NLRP3 expression, surpassing that of the rotenone-treated group (Figs. 3a and 4a). Given this excessive increase in expression, losartan's effect was reassessed at 10 μM, and its results are presented separately (Figs. 3c and 4c). For TLR4 expression, rotenone treatment increases the TLR4 mRNA expression compared to the control group ($P < 0.001$). However, losartan administration could not reverse rotenone's effects, and TLR4 mRNA expression remained significantly higher in the R1+L10 group compared to the control group ($P < 0.01$). Interestingly, 10 μM losartan administration led an increase in TLR4 mRNA expression compared to the control group ($P < 0.05$), but not more than rotenone treatment. Conversely, a combination of 10 μM captopril and rotenone (R1+C10) led to a significant increase in TLR4 mRNA expression compared to the control and the rotenone groups ($P < 0.001$, $P < 0.0001$; respectively), although 10 μM captopril did not induce an increase when administered only (Fig. 3b and d).

Accordingly, rotenone treatment significantly increased the NLRP3 expression compared to the control and L10 groups ($P < 0.01$ for both), while losartan administration decreased ($P < 0.05$). Similar to the losartan groups, rotenone treatment increased the NLRP3 expression compared to the control and C10 groups ($P < 0.001$ for both). For captopril, 100 μM (C100) did not lead to a significant change in NLRP3 expression compared to the control group ($P > 0.05$, Fig. 4b). However, to better evaluate its potential modulatory effects, 10 μM captopril (C10) was also tested (Fig. 4d). Although 10 μM captopril administration could not reverse rotenone's effects in combination groups, 100 μM captopril administration decreased the NLRP3 mRNA expression compared to the rotenone (R1) group ($P < 0.01$).

3.4. Docking analysis of losartan with TLR4

A total of 20 docking poses were generated, and the results are presented in Table 2. The highest binding affinity was observed in the first binding model (ID 1), showing a score of −5.834 kcal/mol, with a root mean square deviation (RMSD) of **0.000 Å** for both the lower bound (L.B.) and upper bound (U.B.). These values indicate the degree of conformational variation among the poses in the same binding cluster. An RMSD of 0.000 Å for both L.B. and U.B. reflects perfect convergence of the docking poses. Other docking models demonstrated binding affinities ranging from −5.808 to −4.953 kcal/mol. A more detailed visualization of the docking interactions, including the binding poses,

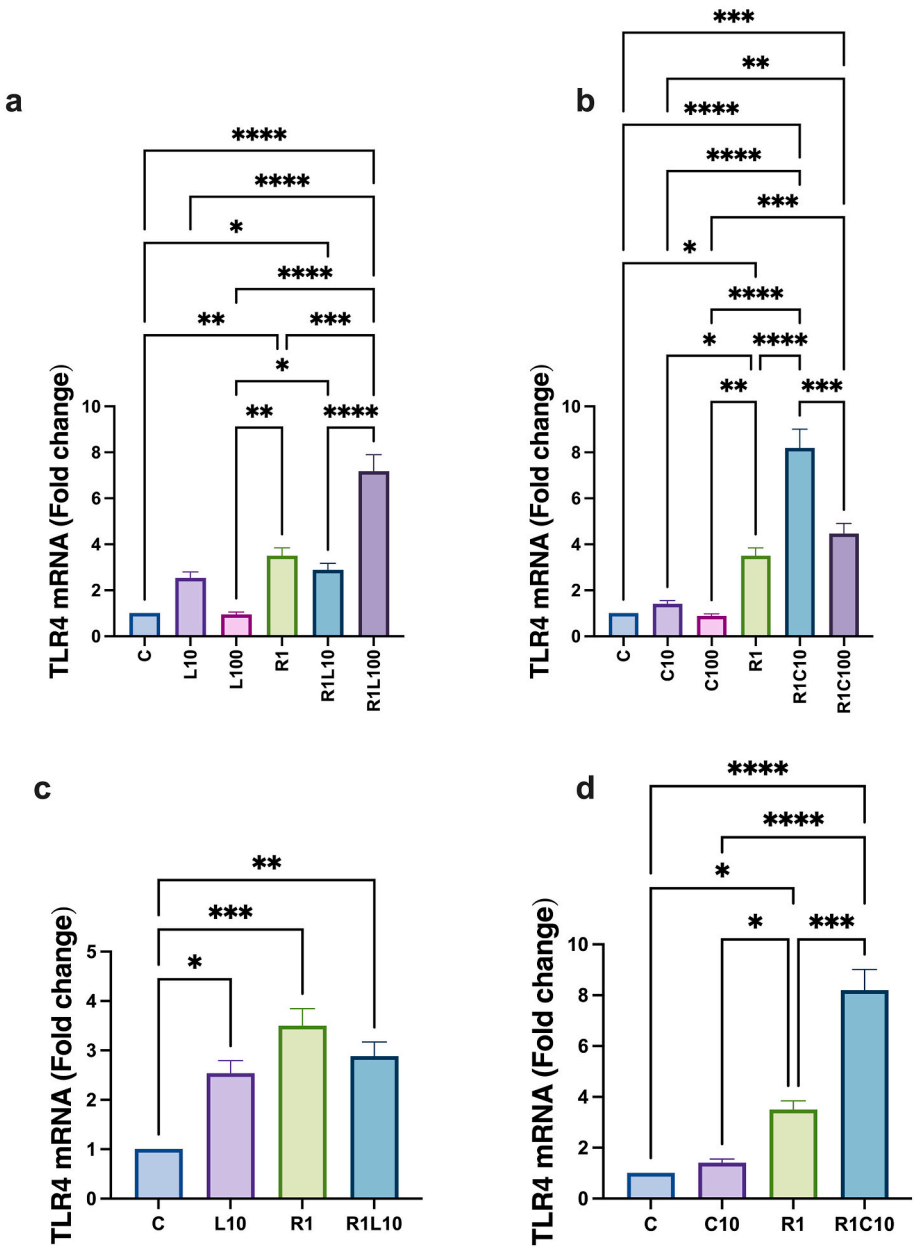

Fig. 3. Fold changes in TLR4 mRNA levels in EGCs. Data were obtained from experiments performed in duplicates and repeated three times. *$p < 0.05$, **$p < 0.01$, ***$p < 0.001$, ***$p < 0.0001$. C: Control, R1: 1 μM Rotenone, C10: 10 μM captopril, C100: 100 μM captopril, L10: 10 μM losartan, L100: 100 μM losartan.

key hydrogen bonds, and van der Waals interactions between losartan and TLR4, is presented in Fig. 5, highlighting the most stable conformation and critical interacting residues.

3.5. Docking analysis of captopril with TLR4

A total of 20 docking poses were generated, and the results are presented in Table 3. The highest binding affinity was observed in the first binding model (ID 1), showing a score of −4.283 kcal/mol, with a root mean square deviation (RMSD) of 0.000 for both the lower bound (L.B.) and upper bound (U.B.). Other docking models demonstrated binding affinities between −4.116 and −3.582 kcal/mol. A more detailed visualization of the docking interactions, including the binding poses, key hydrogen bonds, and van der Waals interactions between captopril and TLR4, is presented in Fig. 6, highlighting the most stable conformation and critical interacting residues.

3.6. Docking analysis of losartan with NLRP3

A total of 18 binding poses were generated, and the results are summarized in Table 4. The best docking score was observed with the first binding model (ID 4.1), which showed a binding affinity of −8.183 kcal/mol and an RMSD value of 0.000 for both lower bound (L.B.) and upper bound (U.B.), indicating a strong and stable interaction. The subsequent models exhibited binding affinities ranging from −8.060 to −7.281 kcal/mol. A more detailed visualization of the docking interactions, including the binding poses, key hydrogen bonds, and van der Waals interactions between losartan and NLRP3, is presented in Fig. 7, highlighting the most stable conformation and critical interacting residues.

3.7. Molecular docking analysis of captopril with NLRP3

A total of 20 binding poses were generated, and the results are

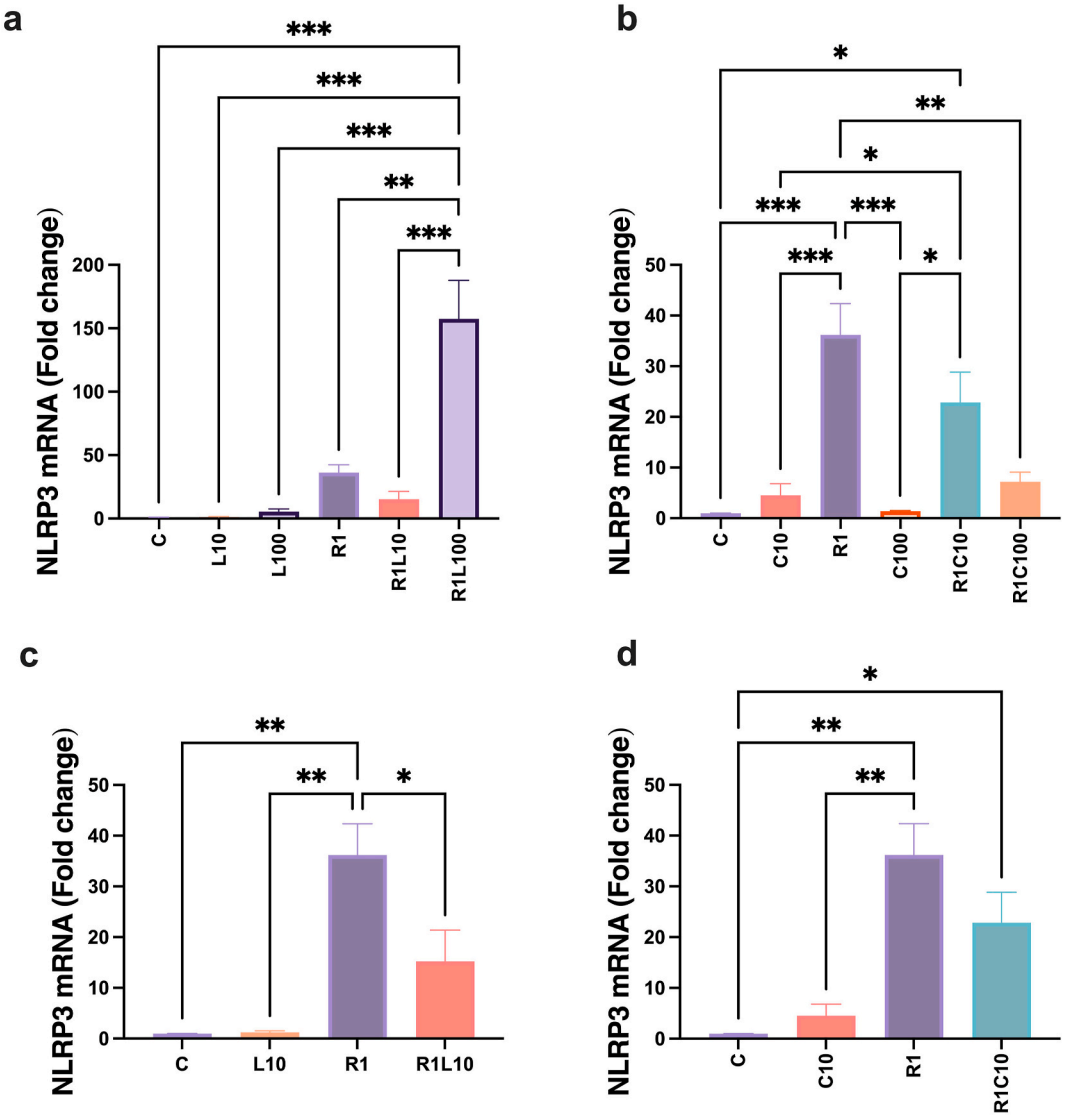

Fig. 4. Fold changes in NLRP3 mRNA levels in EGCs. Data were obtained from experiments performed in duplicates and repeated three times. *$p < 0.05$, **$p < 0.01$. C: Control, R1: 1 μM Rotenone, C10: 10 μM captopril, C100: 100 μM captopril, L10: 10 μM losartan, L100: 100 μM losartan.

summarized in Table 5. The best docking score was observed with the first binding model (ID 1), which showed a binding affinity of −5.347 kcal/mol and a root mean square deviation (RMSD) value of 0.000 for both lower bound (L.B.) and upper bound (U.B.), indicating a strong and stable interaction. The subsequent models exhibited binding affinities ranging from −5.059 to −4.791 kcal/mol. A more detailed visualization of the docking interactions, including the binding poses, key hydrogen bonds, and van der Waals interactions between captopril and NLRP3, is presented in Fig. 8, highlighting the most stable conformation and critical interacting residues.

3.8. Comparative analysis of binding affinities

Molecular docking analyses revealed that losartan exhibited significantly higher binding affinity than captopril toward both target proteins. For TLR4, the average binding energy of losartan was −5.369 kcal/mol (range: −5.834 to −4.953), whereas captopril showed a weaker affinity with a mean score of −3.809 kcal/mol (range: −4.283 to −3.582). Similarly, for NLRP3, losartan demonstrated a substantially stronger affinity (mean: −7.635 kcal/mol; range: −8.183 to −7.281) compared to captopril (mean: −4.933 kcal/mol; range: −5.347 to −4.791).

To further contextualize these findings, TAK-242 (a well-characterized TLR4 inhibitor) and MCC950 (a selective NLRP3 inhibitor) were included as positive controls. TAK-242 showed a mean binding energy of −5.070 kcal/mol (range: −5.361 to −4.781) for TLR4, which was higher than losartan ($p < 0.05$) but lower than captopril ($p < 0.0001$). MCC950 demonstrated the strongest affinity toward NLRP3 among all compounds tested, with a mean binding energy of −8.676 kcal/mol (range: −9.357 to −8.028), exceeding both losartan and captopril ($p < 0.01$ and $p < 0.0001$, respectively).

Taken together, these comparisons suggest that losartan has the potential to act as a dual modulator of TLR4 and NLRP3, with docking scores approaching those of validated inhibitors, whereas captopril exhibits comparatively limited binding capability toward both targets. The comparative results are visualized in Fig. 9. Detailed RMSD and binding affinity scores for TAK-242 (TLR4) and MCC950 (NLRP3) docking poses are provided in Supplementary Tables 1 and 2, respectively.

4. Discussion

In this study, we investigated the effects of losartan and captopril on rotenone-induced inflammation in EGCs, emphasizing the TLR4/NLRP3 signaling pathway through an integrative approach that combined *in*

Table 2
RMSD and binding affinity scores for docking models of losartan with TLR4.

ID	RMSD L.B.	RMSD U.B.	SCORE (kcal/mol)
1	0.000	0.000	−5.834
2	17.509	20.254	−5.808
3	1.811	2.053	−5.633
4	16.819	20.269	−5.566
5	1.684	3.380	−5.521
6	21.260	23.795	−5.497
7	18.175	20.833	−5.436
8	20.728	23.372	−5.386
9	16.121	20.068	−5.371
10	17.800	20.621	−5.351
11	3.699	9.028	−5.334
12	21.268	23.547	−5.325
13	14.750	18.085	−5.318
14	16.314	20.176	−5.254
15	17.324	20.409	−5.254
16	17.589	21.115	−5.232
17	21.109	22.722	−5.208
18	16.206	18.997	−5.115
19	3.881	8.701	−4.984
20	17.272	19.873	−4.953

This table presents the Root Mean Square Deviation (RMSD) lower bound (L.B.), upper bound (U.B.), and the calculated binding affinity scores (in kcal/mol) for the various docking poses of losartan with TLR4. L.B. and U.B. indicate the minimum and maximum RMSD values within each docking cluster, reflecting the conformational variability among poses.

vitro and *in silico* methods. EGCs were chosen due to their functional similarities to astrocytes found in the central nervous system, positioning them at a vital intersection of the gut-brain axis. Given the increasing evidence suggesting that peripheral inflammation originating from the gastrointestinal tract significantly contributes to the initiation and progression of PD, evaluating inflammatory pathways in EGCs provides a physiologically relevant model to investigate disease mechanisms and therapeutic targets. Our findings highlight the potential of losartan and captopril, two clinically approved antihypertensive drugs, to modulate neuroinflammatory pathways implicated in neurodegenerative diseases such as PD.

The RAS, classically identified as a circulating hormonal network controlling blood pressure and electrolyte balance, has more recently been recognized for its significant local regulatory roles within the brain, influencing processes such as oxidative stress, neuroinflammation, and neuronal degeneration (Labandeira-Garcia et al.,

Table 3
RMSD and binding affinity scores for docking models of captopril with TLR4.

ID	RMSD L.B.	RMSD U.B.	SCORE (kcal/mol)
1	0.000	0.000	−4.283
2	2.963	4.011	−4.116
3	19.712	21.377	−3.904
4	1.901	2.374	−3.902
5	1.630	2.270	−3.860
6	20.287	21.308	−3.846
7	20.076	21.429	−3.836
8	3.357	4.463	−3.827
9	19.965	21.334	−3.795
10	1.981	2.198	−3.788
11	19.583	21.027	−3.763
12	19.881	21.353	−3.760
13	2.782	4.724	−3.757
14	2.402	3.383	−3.737
15	11.280	12.907	−3.731
16	17.899	19.502	−3.718
17	18.727	20.274	−3.679
18	3.808	5.553	−3.647
19	19.891	21.246	−3.639
20	7.005	9.405	−3.582

This table presents the Root Mean Square Deviation (RMSD) lower bound (L.B.), upper bound (U.B.), and the calculated binding affinity scores (in kcal/mol) for the various docking poses of captopril with TLR4. L.B. and U.B. indicate the minimum and maximum RMSD values within each docking cluster, reflecting the conformational variability among poses.

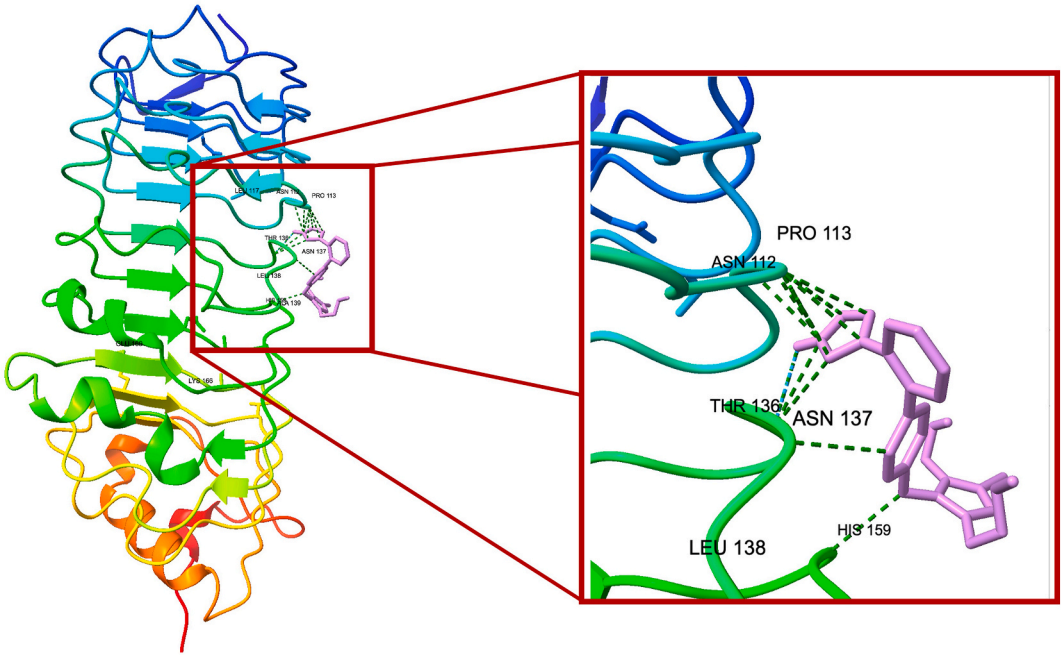

Fig. 5. Binding Mode of the Top-Scoring Docking Model of losartan with TLR4.
This figure illustrates the binding configuration of the highest-affinity docking model for losartan interacting with the TLR4 protein. On the left, the complete 3D structure of TLR4 is displayed, highlighting the losartan binding site. The inset on the right zooms in on the critical binding interactions. Losartan (purple) forms multiple interactions with critical residues of TLR4, including ASN112, PRO113, THR136, ASN112, LEU138, and HIS159. Blue dashed lines indicate hydrogen bonds, while green dashed lines represent van der Waals interactions. These interactions depict the most stable conformation of losartan within the TLR4 binding pocket, as determined by the docking analysis.

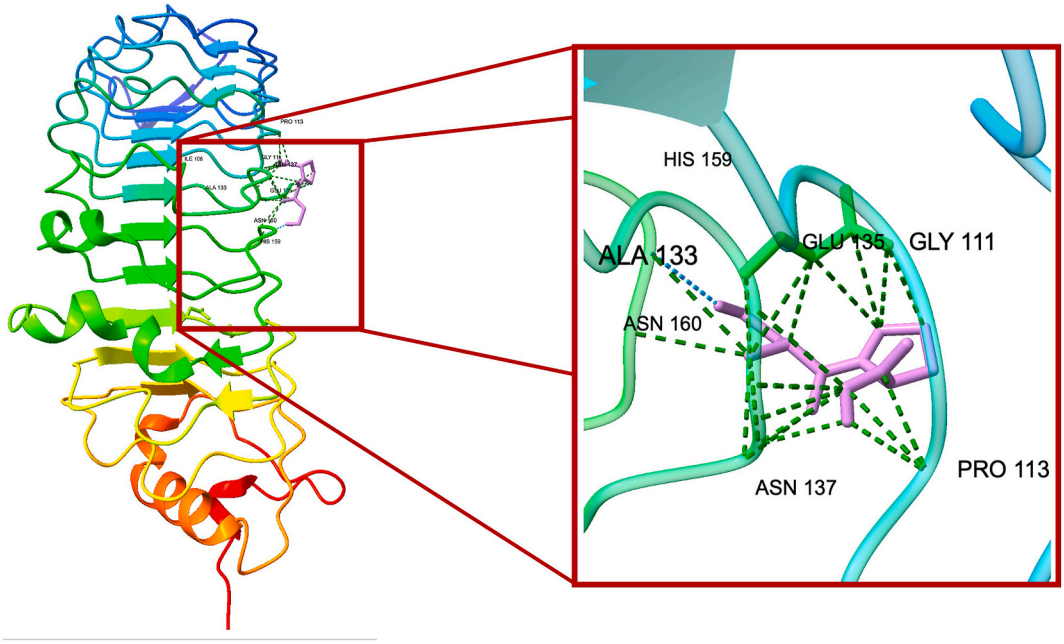

Fig. 6. Binding Mode of the Top-Scoring Docking Model of Captopril with TLR4.
This figure illustrates the binding configuration of the highest-affinity docking model for captopril interacting with the TLR4 protein. On the left, the complete 3D structure of TLR4 is presented, highlighting the captopril binding site. The inset on the right zooms in on the critical binding interactions. Captopril (purple) forms multiple interactions with critical residues of TLR4, including GLY111, PRO113, ALA133, GLU135, ASN137, ASN160, and HIS159. Blue dashed lines indicate hydrogen bonds, while green dashed lines represent van der Waals interactions.These interactions demonstrate the most stable conformation of captopril within the TLR4 binding pocket, as determined by docking analysis.

Table 4
RMSD and binding affinity scores for docking models of losartan with NLRP3.

ID	RMSD L.B.	RMSD U.B.	SCORE (kcal/mol)
1	0.000	0.000	−8.183
2	2.987	7.210	−8.060
3	3.063	7.954	−7.888
4	4.489	9.888	−7.840
5	2.356	2.830	−7.818
6	4.350	9.467	−7.759
7	3.993	6.310	−7.752
8	3.115	7.727	−7.750
9	5.118	8.169	−7.686
10	3.252	7.774	−7.682
11	5.333	8.469	−7.532
12	3.366	8.378	−7.508
13	5.225	8.447	−7.410
14	2.724	7.130	−7.345
15	3.437	8.631	−7.336
16	2.280	3.168	−7.302
17	5.043	10.348	−7.290
18	4.314	6.791	−7.281

This table presents the Root Mean Square Deviation (RMSD) lower bound (L.B.), upper bound (U.B.), and the calculated binding affinity scores (in kcal/mol) for the various docking poses of losartan with NLRP3. L.B. and U.B. indicate the minimum and maximum RMSD values within each docking cluster, reflecting the conformational variability among poses.

2024). Moreover, functional interactions between local dopaminergic signaling and the RAS system have emerged as pivotal in peripheral tissues (Chugh et al., 2012; Yang et al., 2012) and increasingly within the brain (Labandeira-Garcia et al., 2024). Imbalanced interactions between these two systems have been associated with neurodegenerative disorders, particularly PD, where alterations in dopaminergic neurotransmission are considered a fundamental pathogenic characteristic (Kobiec et al., 2021). Since the therapies currently available for neurodegenerative diseases focus on alleviating symptoms, finding drugs that can modify the disease itself is a crucial priority (Perez-Lloret et al., 2017). In this respect, modulating angiotensin-related inflammatory signaling in peripheral cell types, such as EGCs, may provide novel insights into therapeutic approaches targeting early neuroinflammatory processes in PD pathology.

Consistent with prior literature (Salmani et al., 2018; Sepehri et al., 2016; Wang et al., 2019), losartan exhibited a potent inhibitory effect on inflammation, significantly reducing rotenone-induced caspase-1 levels. Interestingly, a previous study demonstrated that angiotensin II itself could exert protective effects on dopaminergic neurons against rotenone-induced toxicity via the AT2 receptor subtype, whereas simultaneous inhibition of AT1 receptors by losartan further enhanced neuroprotection, indicating receptor subtype selectivity and differential downstream signaling as critical determinants in neuroprotection (Grammatopoulos et al., 2005). Given these observations, the protective effect of losartan against inflammation observed in our model could similarly be attributed to selective AT1 receptor blockade, which may potentially shift the balance toward beneficial signaling pathways involving AT2 receptor activation. Indeed, previous studies have shown that AT1 receptor blockade can potentiate AT2 receptor signaling, thereby exerting anti-inflammatory, vasodilatory, and neuroprotective effects (Bregonzio et al., 2008; Naito et al., 2010).

Captopril, an ACE inhibitor, has also exhibited prominent anti-inflammatory effects through inhibiting Nuclear Factor kappa B (NF-κB) (Gan et al., 2018). Therefore, the neuroprotective activity of captopril has been confirmed in experimental models of PD (Sonsalla et al., 2013), memory impairment (Abareshi et al., 2016) and AD (Ishola et al., 2022). Although captopril did not significantly decrease caspase-1 levels induced by rotenone, its mild inhibitory trend aligns with previously reported anti-inflammatory properties (Bryniarski et al., 2021; Peeters et al., 1998). Interestingly, both losartan and captopril treatments, when administered alone, paradoxically increased caspase-1 compared to controls. Although the precise mechanisms behind these unexpected pro-inflammatory effects remain unclear, similar paradoxical effects of anti-inflammatory drugs at specific concentrations or contexts have been previously documented (Doux et al., 2005; Rhein

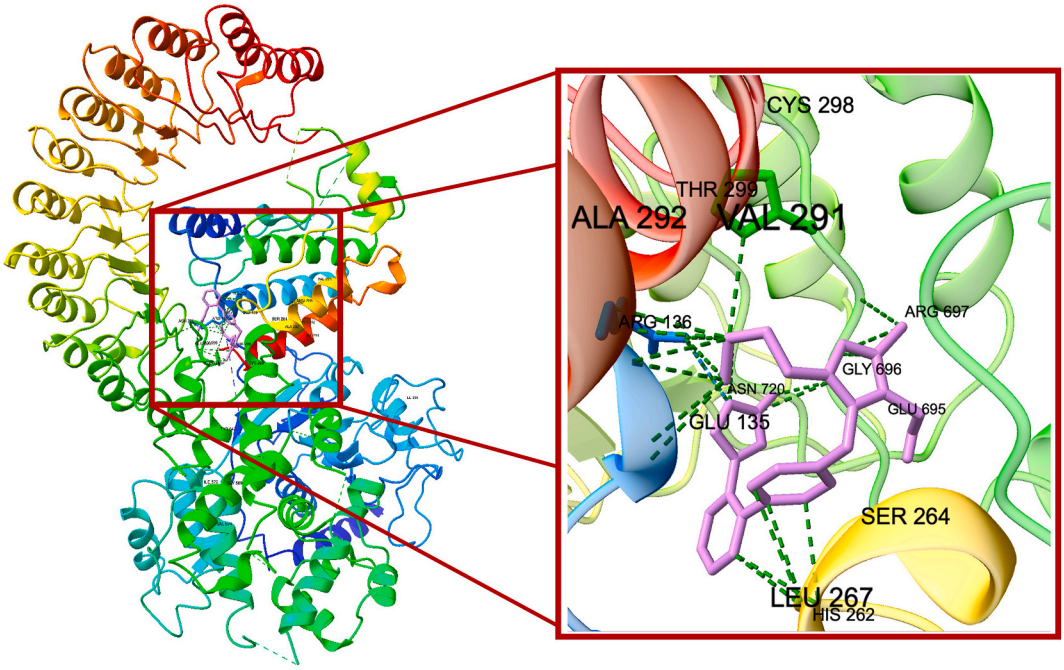

Fig. 7. Binding Mode of the Top-Scoring Docking Model of Losartan with NLRP3.
This figure illustrates the binding configuration of the highest-affinity docking model for losartan interacting with the NLRP3 complex. On the left, the complete 3D structure of NLRP3 is presented, highlighting the losartan binding site. The inset on the right zooms in on the critical binding interactions. Losartan (purple) forms multiple interactions with critical residues of NLRP3, including ARG136, GLU135, ASN720, GLY696, GLU695, SER264, LEU267, HIS262, THR299, ALA292, VAL291 and CYS298. Blue dashed lines indicate hydrogen bonds, while green dashed lines represent van der Waals interactions. These interactions demonstrate the most stable conformation of captopril within the TLR4 binding pocket, as determined by docking analysis.

Table 5
RMSD and binding affinity scores for docking models of captopril with NLRP3.

ID	RMSD L.B.	RMSD U.B.	SCORE (kcal/mol)
1	0.000	0.000	−5.347
2	19.556	20.506	−5.059
3	17.664	19.100	−5.054
4	17.993	19.297	−5.019
5	17.396	18.813	−4.974
6	16.998	18.471	−4.964
7	17.058	18.537	−4.947
8	20.034	20.843	−4.941
9	17.561	18.898	−4.937
10	19.729	21.102	−4.930
11	18.019	19.355	−4.923
12	18.905	20.179	−4.901
13	18.904	20.289	−4.899
14	20.932	22.215	−4.884
15	14.751	16.369	−4.845
16	17.766	19.028	−4.834
17	18.268	19.665	−4.813
18	3.675	5.247	−4.803
19	18.379	19.800	−4.801
20	16.246	17.644	−4.791

This table presents the Root Mean Square Deviation (RMSD) lower bound (L.B.), upper bound (U.B.), and the calculated binding affinity scores (in kcal/mol) for the various docking poses of captopril with NLRP3. L.B. and U.B. indicate the minimum and maximum RMSD values within each docking cluster, reflecting the conformational variability among poses.

et al., 2024), suggesting possible receptor-mediated compensatory responses or off-target inflammatory activation pathways. In particular, the significant increase in cell proliferation observed with 1000 μM captopril may reflect a biphasic dose-response effect. Previous studies have shown that captopril exhibits a biphasic inhibitory profile in endothelial cell migration (Volpert et al., 1996) and in the brain and vascular system (Unger et al., 1981). Such a biphasic phenomenon may underlie the proliferative effects observed in our model at high concentrations.

The complexity of the cytokine responses was evident, with IL-1β expression not significantly altered by treatments in this study. Although caspase-1 activation typically governs IL-1β maturation and release (Conos et al., 2016), the unchanged IL-1β levels observed in our experimental conditions may reflect differential cellular responses, and the requirement of additional inflammasome components governing cytokine release (Netea et al., 2009). Indeed, our findings showing altered NLRP3 mRNA expression suggest that while inflammasome priming and initiation via NLRP3 are clearly affected by rotenone and modulated by losartan and captopril, subsequent steps necessary for IL-1β secretion may not have been sufficiently activated or might have been differentially regulated under these specific experimental conditions.

Angiotensin II Type 1 Receptor 1 (AT1R) blockage has been shown to be antiinflammatory in different diseases, including stroke (Sironi et al., 2004) and PD (Joglar et al., 2009). Losartan has been shown to attenuate neuroinflammation in various models, including neuropathic pain (Kalynovska et al., 2020), AD (Danielyan et al., 2010), and systemic inflammation (Drews et al., 2019). It reduces the expression of pro-inflammatory cytokines (Abdul-Muneer et al., 2018; Kim et al., 2019). Losartan effectively inhibits TLR4 expression across various tissues, contributing to its anti-inflammatory and protective effects in conditions like hypertension, renal and liver fibrosis (De Batista et al., 2014; Ni et al., 2012). Similarly, captopril has been reported to inhibit TLR4 expression in adipose tissue (Mitchell et al., 2021). However, in our study, the observed modulation of TLR4 mRNA expression further highlighted the complexity of inflammatory regulation. Rotenone treatment, as expected, significantly increased TLR4 expression, aligning with its known pro-inflammatory properties via pattern recognition receptors like TLR4. Interestingly, neither losartan nor captopril was able to fully reverse the rotenone-induced upregulation of TLR4 expression. Furthermore, 10 μM losartan alone significantly elevated

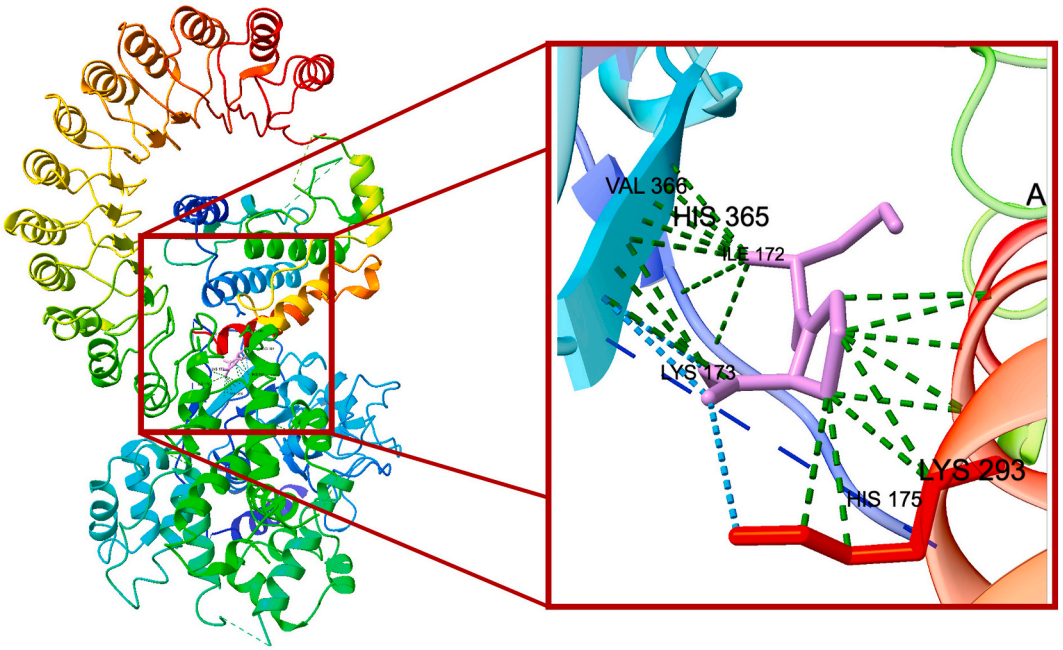

Fig. 8. Binding Mode of the Top-Scoring Docking Model of Captopril with NLRP3.
This figure illustrates the binding configuration of the highest-affinity docking model for captopril interacting with the NLRP3 complex. On the left, the complete 3D structure of NLRP3 is presented, highlighting the captopril binding site. The inset on the right zooms in on the critical binding interactions. Captopril (purple) forms multiple interactions with critical residues of NLRP3, including LYS173, HIS175, LYS293, ILE172, HIS365, and VAL366. Blue dashed lines indicate hydrogen bonds, while green dashed lines represent van der Waals interactions. These interactions demonstrate the most stable conformation of captopril within the TLR4 binding pocket, as determined by docking analysis.

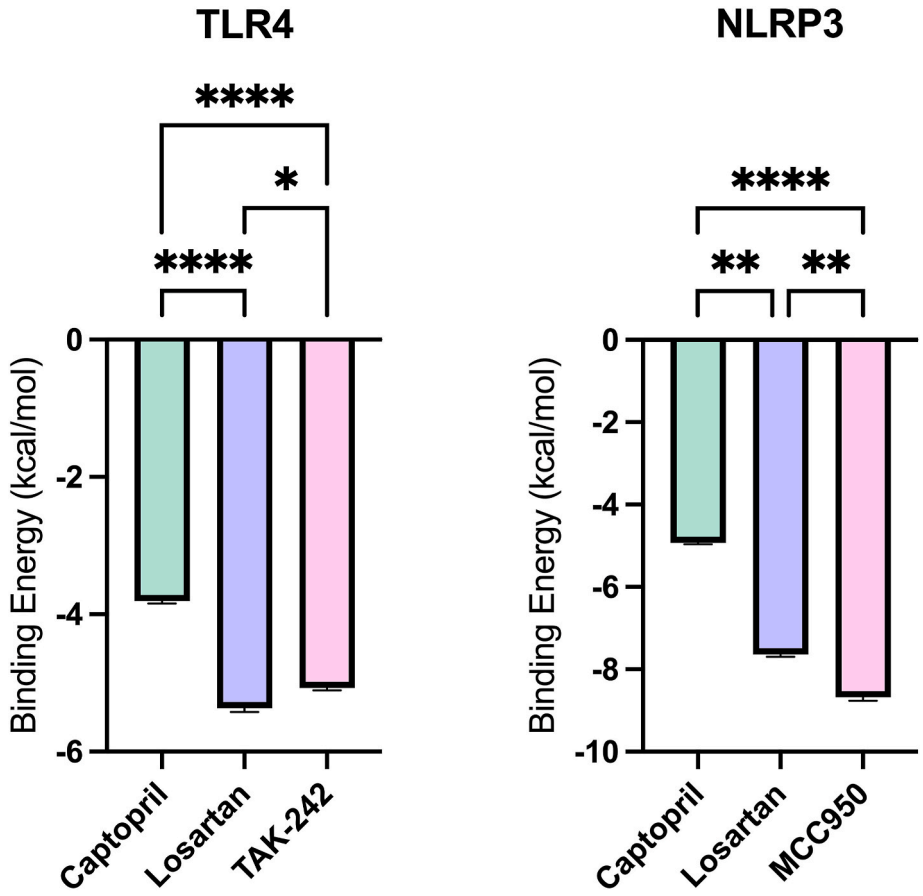

Fig. 9. Comparison of binding energies (kcal/mol) of captopril, losartan, and positive control compounds to TLR4 (left) and NLRP3 (right) proteins. Data represent mean ± SEM. ****$p < 0.0001$.

TLR4 expression compared to control, indicating that even at low concentrations, losartan may paradoxically activate or sensitize inflammatory pathways under certain cellular conditions. Similarly, captopril combined with rotenone further potentiated TLR4 upregulation beyond rotenone treatment alone, despite captopril alone being inert. The observed modulation of TLR4 mRNA expression highlights the dual and context-dependent role of TLR4 signaling in inflammation (Heine and Zamyatina, 2022). Under physiological conditions, controlled activation of TLR4 contributes beneficially to innate immune responses, aiding in pathogen clearance and maintaining tissue homeostasis (Oda et al., 2024). Conversely, persistent or excessive activation can lead to chronic inflammatory states, contributing to inflammatory disease progression (Lucas and Maes, 2013). Consistent with this dual functionality, recent literature suggests therapeutic potential for TLR4 agonists in AD through controlled stimulation of the immune system to facilitate clearance of amyloid-beta (Michaud et al., 2013). Therefore, the paradoxical increase of TLR4 expression following losartan or captopril treatments observed in our study likely reflects such complex regulatory dynamics. In parallel with our findings on TLR4 expression, NLRP3 inflammasome signaling exhibited distinct and concentration-dependent modulation by losartan and captopril. Specifically, losartan at a lower concentration (10 μM) significantly decreased NLRP3 mRNA expression, suggesting effective suppression of inflammasome priming at this dose. In contrast, captopril required a higher concentration (100 μM) to significantly reduce NLRP3 expression, indicating a potential difference in potency or pharmacological profiles between the two drugs regarding inflammasome inhibition.

The observed upregulation of TLR4 mRNA expression following treatment with losartan and captopril, both alone and in combination with rotenone, presents a complex picture. While AT1R blockage by losartan is generally considered anti-inflammatory, the paradoxical increase in TLR4 expression suggests the involvement of compensatory mechanisms or off-target effects (Regan et al., 2019; Strauss and Hall, 2006). Blockade of AT1R can lead to an increase in angiotensin II levels due to the removal of negative feedback on renin release which then interacted with angiotensin II Type 2 Receptor (AT2R), that could potentially contribute to TLR4 upregulation in specific cellular contexts (Nakashima et al., 2015; Otsui et al., 2007). Similarly, captopril's potentiation of rotenone-induced TLR4 upregulation at 10 μM, despite being inert on its own, highlights the complexity of its interaction with inflammatory pathways in this specific cellular environment. This could involve its effects on bradykinin levels or other downstream targets of ACE inhibition (Anning et al., 1995). Moreover, the interplay between the drug and the rotenone-induced inflammatory environment might further contribute to the observed paradoxical effects. Rotenone's known pro-inflammatory properties could create a cellular state where the addition of losartan or captopril triggers unexpected responses in TLR4 expression.

Docking analyses complemented these biochemical findings by elucidating the molecular basis of interaction between the studied drugs and the TLR4/NLRP3 proteins. Losartan demonstrated strong binding affinity to TLR4 and NLRP3 proteins, surpassing captopril's binding affinity. The identified key residues provide molecular insight into the inhibitory actions of losartan, suggesting that the observed biological effects might arise through stabilizing receptor conformations that impede downstream signaling cascades. For TLR4, losartan exhibited a stronger binding affinity than TAK-242, a well-characterized TLR4 inhibitor, suggesting that it may directly interfere with TLR4-mediated signaling with comparable or even superior efficacy. For NLRP3, losartan demonstrated high affinity, although not exceeding that of MCC950, a potent and selective NLRP3 inhibitor. Nonetheless, its binding profile was close enough to suggest a plausible mechanistic role in modulating inflammasome activation. In contrast, the lower binding affinity observed for captopril suggests a reduced capacity to modulate these receptors directly, which correlates with the modest biochemical effects observed. Nonetheless, despite its lower affinity, captopril's potential modulatory effects observed biochemically cannot be disregarded.

The current study has some limitations. First, while molecular docking analyses provide critical insights into potential drug-target interactions, these findings necessitate validation through more detailed molecular dynamics simulations and *in vivo* models to confirm their physiological relevance and therapeutic potential. Additionally, the complexity of neuroinflammatory signaling networks extends beyond the TLR4/NLRP3 pathway, suggesting that complementary pathways such as NF-κB or other inflammasomes may also significantly contribute to the observed cellular effects.

In conclusion, our integrative *in vitro* and *in silico* study provides compelling evidence that losartan and captopril exhibit promising inhibitory effects on rotenone-induced neuroinflammation via modulation of the TLR4/NLRP3 pathway. This underlines their potential for repurposing as neuroprotective agents in diseases characterized by neuroinflammation, particularly PD. However, further studies are needed to elucidate the complex and context-dependent actions of these drugs and establish efficacy, safety, and optimal dosing strategies.

Declaration of competing interest

The authors declare that there are no conflicts of interest.

Appendix A. Supplementary data

Supplementary data to this article can be found online at https://doi.org/10.1016/j.ejphar.2025.177932.

Data availability

Data will be made available on request.

References

Abareshi, A., Hosseini, M., Beheshti, F., Norouzi, F., Khazaei, M., Sadeghnia, H.R., Boskabady, M.H., Shafei, M.N., Anaeigoudari, A., 2016. The effects of captopril on lipopolysaccharide induced learning and memory impairments and the brain cytokine levels and oxidative damage in rats. Life Sci. 167, 46–56.
Abdul-Muneer, P.M., Bhowmick, S., Briski, N., 2018. Angiotensin II causes neuronal damage in stretch-injured neurons: protective effects of Losartan, an angiotensin T (1) receptor blocker. Mol. Neurobiol. 55, 5901–5912.
Anning, P.B., Grocott-Mason, R.M., Lewis, M.J., Shah, A.M., 1995. Enhancement of left ventricular relaxation in the isolated heart by an angiotensin-converting enzyme inhibitor. Circulation 92, 2660–2665.
Bonaz, B., 2024. The gut-brain axis in Parkinson's disease. Rev. Neurol. 180, 65–78.
Bregonzio, C., Seltzer, A., Armando, I., Pavel, J., Saavedra, J.M., 2008. Angiotensin II AT (1) receptor blockade selectively enhances brain AT(2) receptor expression, and abolishes the cold-restraint stress-induced increase in tyrosine hydroxylase mRNA in the locus coeruleus of spontaneously hypertensive rats. Stress 11, 457–466.
Brudek, T., 2019. Inflammatory bowel diseases and Parkinson's Disease. J. Parkinsons Dis. 9, S331–s344.
Bryniarski, P., Nazimek, K., Marcinkiewicz, J., 2021. Anti-inflammatory activities of captopril and diuretics on macrophage activity in mouse humoral immune response. Int. J. Mol. Sci. 22.
Chugh, G., Lokhandwala, M.F., Asghar, M., 2012. Altered functioning of both renal dopamine D1 and angiotensin II type 1 receptors causes hypertension in old rats. Hypertension 59, 1029–1036.
Cirillo, C., Sarnelli, G., Esposito, G., Turco, F., Steardo, L., Cuomo, R., 2011. S100B protein in the gut: the evidence for enteroglial-sustained intestinal inflammation. World J. Gastroenterol. 17, 1261–1266.
Coll, R.C., Hill, J.R., Day, C.J., Zamoshnikova, A., Boucher, D., Massey, N.L., Chitty, J.L., Fraser, J.A., Jennings, M.P., Robertson, A.A.B., Schroder, K., 2019. MCC950 directly targets the NLRP3 ATP-hydrolysis motif for inflammasome inhibition. Nat. Chem. Biol. 15, 556–559.
Conos, S.A., Lawlor, K.E., Vaux, D.L., Vince, J.E., Lindqvist, L.M., 2016. Cell death is not essential for caspase-1-mediated interleukin-1β activation and secretion. Cell Death Differ. 23, 1827–1838.
Danielyan, L., Klein, R., Hanson, L.R., Buadze, M., Schwab, M., Gleiter, C.H., Frey, W.H., 2010. Protective effects of intranasal losartan in the APP/PS1 transgenic mouse model of alzheimer disease. Rejuvenation Res. 13, 195–201.
De Batista, P.R., Palacios, R., Martín, A., Hernanz, R., Médici, C.T., Silva, M.A., Rossi, E. M., Aguado, A., Vassallo, D.V., Salaices, M., Alonso, M.J., 2014. Toll-like receptor 4 upregulation by angiotensin II contributes to hypertension and vascular dysfunction through reactive oxygen species production. PLoS One 9, e104020.

Doux, J.D., Bazar, K.A., Lee, P.Y., Yun, A.J., 2005. Can chronic use of anti-inflammatory agents paradoxically promote chronic inflammation through compensatory host response? Med. Hypotheses 65, 389–391.
Drews, H.J., Yenkoyan, K., Lourhmati, A., Buadze, M., Kabisch, D., Verleysdonk, S., Petschak, S., Beer-Hammer, S., Davtyan, T., Frey 2nd, W.H., Gleiter, C.H., Schwab, M., Danielyan, L., 2019. Intranasal losartan decreases perivascular beta amyloid, inflammation, and the decline of neurogenesis in hypertensive rats. Neurotherapeutics 16, 725–740.
Espitia-Corredor, J.A., Boza, P., Espinoza-Pérez, C., Lillo, J.M., Rimassa-Taré, C., Machuca, V., Osorio-Sandoval, J.M., Vivar, R., Bolivar, S., Pardo-Jiménez, V., Sánchez-Ferrer, C.F., Peiró, C., Díaz-Araya, G., 2022. Angiotensin II triggers NLRP3 inflammasome activation by a Ca(2+) signaling-dependent pathway in rat cardiac fibroblast Ang-II by a Ca(2+)-Dependent mechanism triggers NLRP3 inflammasome in CF. Inflammation 45, 2498–2512.
Gan, Z., Huang, D., Jiang, J., Li, Y., Li, H., Ke, Y., 2018. Captopril alleviates hypertension-induced renal damage, inflammation, and NF-κB activation. Braz. J. Med. Biol. Res. 51, e7338.
Garrido-Gil, P., Rodriguez-Perez, A.I., Dominguez-Meijide, A., Guerra, M.J., Labandeira-Garcia, J.L., 2018. Bidirectional neural interaction between central dopaminergic and gut lesions in Parkinson's disease models. Mol. Neurobiol. 55, 7297–7316.
Gorecki, A.M., Anyaegbu, C.C., Anderton, R.S., 2021. TLR2 and TLR4 in Parkinson's disease pathogenesis: the environment takes a toll on the gut. Transl. Neurodegener. 10, 47.
Grammatopoulos, T.N., Ahmadi, F., Jones, S.M., Fariss, M.W., Weyhenmeyer, J.A., Zawada, W.M., 2005. Angiotensin II protects cultured midbrain dopaminergic neurons against rotenone-induced cell death. Brain Res. 1045, 64–71.
Grela, E., Kozłowska, J., Grabowiecka, A., 2018. Current methodology of MTT assay in bacteria – a review. Acta Histochem. 120, 303–311.
Heine, H., Zamyatina, A., 2022. Therapeutic targeting of TLR4 for inflammation, infection, and cancer: a perspective for disaccharide lipid A mimetics. Pharmaceuticals 16.
Houser, M.C., Tansey, M.G., 2017. The gut-brain axis: is intestinal inflammation a silent driver of Parkinson's disease pathogenesis? npj Parkinson's Dis. 3, 3.
Ishola, I., Afolayan, O., Badru, A., Olubodun-Obadun, T., John, N., Adeyemi, O., 2022. Angiotensin converting enzyme inhibitor captopril prevents neuronal overexpression of amyloid-beta and alpha-synuclein in Drosophila melanogaster genetic models of neurodegenerative diseases. Niger. J. Physiol. Sci. 37, 21–28.
Joglar, B., Rodriguez-Pallares, J., Rodriguez-Perez, A.I., Rey, P., Guerra, M.J., Labandeira-Garcia, J.L., 2009. The inflammatory response in the MPTP model of Parkinson's disease is mediated by brain angiotensin: relevance to progression of the disease. J. Neurochem. 109, 656–669.
Kalynovska, N., Diallo, M., Sotakova-Kasparova, D., Palecek, J., 2020. Losartan attenuates neuroinflammation and neuropathic pain in paclitaxel-induced peripheral neuropathy. J. Cell Mol. Med. 24, 7949–7958.
Kielian, T., 2006. Toll-like receptors in central nervous system glial inflammation and homeostasis. J. Neurosci. Res. 83, 711–730.
Kim, E., Hwang, S.H., Kim, H.K., Abdi, S., Kim, H.K., 2019. Losartan, an angiotensin II type 1 receptor antagonist, alleviates mechanical hyperalgesia in a rat model of chemotherapy-induced neuropathic pain by inhibiting inflammatory cytokines in the dorsal root ganglia. Mol. Neurobiol. 56, 7408–7419.
Kobiec, T., Otero-Losada, M., Chevalier, G., Udovin, L., Bordet, S., Menéndez-Maissonave, C., Capani, F., Pérez-Lloret, S., 2021. The renin–angiotensin system modulates dopaminergic neurotransmission: a new player on the scene. Front. Synaptic Neurosci. 13.
Labandeira-Garcia, J.L., Labandeira, C.M., Guerra, M.J., Rodriguez-Perez, A.I., 2024. The role of the brain renin-angiotensin system in parkinson's disease. Transl. Neurodegener. 13, 22.
Lucas, K., Maes, M., 2013. Role of the toll like receptor (TLR) radical cycle in chronic inflammation: possible treatments targeting the TLR4 pathway. Mol. Neurobiol. 48, 190–204.
Matsunaga, N., Tsuchimori, N., Matsumoto, T., Ii, M., 2011. TAK-242 (resatorvid), a small-molecule inhibitor of toll-like receptor (TLR) 4 signaling, binds selectively to TLR4 and interferes with interactions between TLR4 and its adaptor molecules. Mol. Pharmacol. 79, 34–41.
Michaud, J.P., Hallé, M., Lampron, A., Thériault, P., Préfontaine, P., Filali, M., Tribout-Jover, P., Lanteigne, A.M., Jodoin, R., Cluff, C., Brichard, V., Palmantier, R., Pilorget, A., Larocque, D., Rivest, S., 2013. Toll-like receptor 4 stimulation with the detoxified ligand monophosphoryl lipid A improves Alzheimer's disease-related pathology. Proc. Natl. Acad. Sci. U. S. A. 110, 1941–1946.
Mitchell, C.S., Premaratna, S.D., Bennett, G., Lambrou, M., Stahl, L.A., Jois, M., Barber, E., Antoniadis, C.P., Woods, S.C., Cameron-Smith, D., Weisinger, R.S., Begg, D.P., 2021. Inhibition of the renin-angiotensin system reduces gene expression of inflammatory mediators in adipose tissue independent of energy balance. Front. Endocrinol. 12, 682726.
Montanari, M., Imbriani, P., Bonsi, P., Martella, G., Peppe, A., 2023. Beyond the microbiota: understanding the role of the enteric nervous system in parkinson's disease from mice to human. Biomedicines 11, 1560.
Naito, T., Ma, L.J., Yang, H., Zuo, Y., Tang, Y., Han, J.Y., Kon, V., Fogo, A.B., 2010. Angiotensin type 2 receptor actions contribute to angiotensin type 1 receptor blocker effects on kidney fibrosis. Am. J. Physiol. Ren. Physiol. 298, F683–F691.
Nakashima, T., Umemoto, S., Yoshimura, K., Matsuda, S., Itoh, S., Murata, T., Fukai, T., Matsuzaki, M., 2015. TLR4 is a critical regulator of angiotensin II-induced vascular remodeling: the roles of extracellular SOD and NADPH oxidase. Hypertens. Res. 38, 649–655.
Netea, M.G., Nold-Petry, C.A., Nold, M.F., Joosten, L.A., Opitz, B., van der Meer, J.H., van de Veerdonk, F.L., Ferwerda, G., Heinhuis, B., Devesa, I., Funk, C.J., Mason, R.J., Kullberg, B.J., Rubartelli, A., van der Meer, J.W., Dinarello, C.A., 2009. Differential requirement for the activation of the inflammasome for processing and release of IL-1beta in monocytes and macrophages. Blood 113, 2324–2335.
Ni, S., Li, Y., Huang, S., Luo, W., Li, C., Li, X., 2012. [perindopril and losartan attenuate intrahepatic toll-like receptor 4 protein expression in rats with bile duct ligation-induced hepatic fibrosis]. Nan Fang Yi Ke Da Xue Xue Bao 32, 211–214.
Oda, M., Yamamoto, H., Kawakami, T., 2024. Maintenance of homeostasis by TLR4 ligands. Front. Immunol. 15, 1286270.
Otsui, K., Inoue, N., Kobayashi, S., Shiraki, R., Honjo, T., Takahashi, M., Hirata, K.-i., Kawashima, S., Yokoyama, M., 2007. Enhanced expression of TLR4 in smooth muscle cells in human atherosclerotic coronary arteries. Heart Vessel. 22, 416–422.
Peeters, A.C., Netea, M.G., Kullberg, B.J., Thien, T., van der Meer, J.W., 1998. The effect of renin-angiotensin system inhibitors on pro- and anti-inflammatory cytokine production. Immunology 94, 376–379.
Perez-Lloret, S., Otero-Losada, M., Toblli, J.E., Capani, F., 2017. Renin-angiotensin system as a potential target for new therapeutic approaches in parkinson's disease. Expet Opin. Invest. Drugs 26, 1163–1173.
Perez-Pardo, P., Dodiya, H., Engen, P., Forsyth, C., Huschens, A., Shaikh, M., Voigt-Zuwala, R., Naqib, A., Green, S., Kordower, J., Shannon, K., Garssen, J., Kraneveld, A., Keshavarzian, A., 2018. Role of TLR4 in the gut-brain axis in Parkinson's disease: a translational study from men to mice. Gut 68 gutjnl-2018.
Rabaneda-Lombarte, N., Blasco-Agell, L., Serratosa, J., Ferigle, L., Saura, J., Solà, C., 2020. Parkinsonian neurotoxicants impair the anti-inflammatory response induced by IL4 in glial cells: involvement of the CD200-CD200R1 ligand-receptor pair. Sci. Rep. 10, 10650.
Rabaneda-Lombarte, N., Xicoy-Espaulella, E., Serratosa, J., Saura, J., Solà, C., 2019. Parkinsonian neurotoxins impair the pro-inflammatory response of glial cells. Front. Mol. Neurosci. 11, 479.
Regan, D.P., Coy, J.W., Chahal, K.K., Chow, L., Kurihara, J.N., Guth, A.M., Kufareva, I., Dow, S.W., 2019. The angiotensin receptor Blocker Losartan suppresses growth of pulmonary metastases via AT1R-Independent inhibition of CCR2 signaling and Monocyte recruitment. J. Immunol. 202, 3087–3102.
Rhein, C., Apelt, I., Werner, F., Schäflein, E., Adler, W., Reichel, M., Schug, C., Morawa, E., Erim, Y., 2024. Paradoxical effect of anti-inflammatory drugs on IL-6 mRNA expression in patients with PTSD during treatment. J. Neural Transm. 131, 813–821.
Salmani, H., Hosseini, M., Beheshti, F., Baghcheghi, Y., Sadeghnia, H.R., Soukhtanloo, M., Shafei, M.N., Khazaei, M., 2018. Angiotensin receptor blocker, losartan ameliorates neuroinflammation and behavioral consequences of lipopolysaccharide injection. Life Sci. 203, 161–170.
Samur, D.N., Yıldırım, S., Maytalman, E., Kalay, M., Tanrıöver, G., Özbey, G., 2025. Vortioxetine attenuates rotenone-induced enteric neuroinflammation via modulation of the TLR2/S100B/RAGE signaling pathway in a rat model of Parkinson's disease. Neuropharmacology 271, 110385.
Santhosh, S., Zanoletti, L., Stamp, L.A., Hao, M.M., Matteoli, G., 2024. From diversity to disease: unravelling the role of enteric glial cells. Front. Immunol. 15, 1408744.
Sepehri, Z., Masoumi, M., Ebrahimi, N., Kiani, Z., Nasiri, A.A., Kohan, F., Sheikh Fathollahi, M., Kazemi Arababadi, M., Asadikaram, G., 2016. Atorvastatin, Losartan and Captopril lead to upregulation of TGF-β, and downregulation of IL-6 in coronary artery disease and hypertension. PLoS One 11, e0168312.
Sironi, L., Gelosa, P., Guerrini, U., Banfi, C., Crippa, V., Brioschi, M., Gianazza, E., Nobili, E., Gianella, A., de Gasparo, M., Tremoli, E., 2004. Anti-Inflammatory effects of AT1 receptor blockade provide end-organ protection in stroke-prone rats independently from blood pressure fall. J. Pharmacol. Exp. Therapeut. 311, 989–995.
Sonsalla, P.K., Coleman, C., Wong, L.Y., Harris, S.L., Richardson, J.R., Gadad, B.S., Li, W., German, D.C., 2013. The angiotensin converting enzyme inhibitor captopril protects nigrostriatal dopamine neurons in animal models of parkinsonism. Exp. Neurol. 250, 376–383.
Strauss, M.H., Hall, A.S., 2006. Angiotensin receptor blockers may increase risk of myocardial infarction: unraveling the ARB-MI paradox. Circulation 114, 838–854.
Suleiman Khoury, Z., Sohail, F., Wang, J., Mendoza, M., Raake, M., Tahoor Silat, M., Reddy Bathinapatta, M., Sadeghzadegan, A., Meghana, P., Paul, J., 2024. Neuroinflammation: a critical factor in neurodegenerative disorders. Cureus 16, e62310.
Tamura, K., Kanaoka, T., Kobayashi, R., Ohki, K., Ohsawa, M., 2015. TLR4 as a possible key regulator of pathological vascular remodeling by Ang II receptor activation. Hypertens. Res. 38, 642–643.
Umer, H., Sharif, A., Khan, H.M., Anjum, S.M.M., Akhtar, B., Ali, S., Ali, M., Hanif, M.A., 2025. Mitigation of neuroinflammation and oxidative stress in rotenone-induced parkinson mouse model through liposomal Coenzyme-Q10 intervention: a comprehensive In-vivo Study. Inflammation.
Unger, T., Kaufmann-Bühler, I., Schölkens, B., Ganten, D., 1981. Brain converting enzyme inhibition: a possible mechanism for the antihypertensive action of captopril in spontaneously hypertensive rats. Eur. J. Pharmacol. 70, 467–478.
Villarán, R.F., Espinosa-Oliva, A.M., Sarmiento, M., De Pablos, R.M., Argüelles, S., Delgado-Cortés, M.J., Sobrino, V., Van Rooijen, N., Venero, J.L., Herrera, A.J., Cano, J., Machado, A., 2010. Ulcerative colitis exacerbates lipopolysaccharide-induced damage to the nigral dopaminergic system: potential risk factor in parkinson's disease. J. Neurochem. 114, 1687–1700.
Volpert, O.V., Ward, W.F., Lingen, M.W., Chesler, L., Solt, D.B., Johnson, M.D., Molteni, A., Polverini, P.J., Bouck, N.P., 1996. Captopril inhibits angiogenesis and slows the growth of experimental tumors in rats. J. Clin. Investig. 98, 671–679.
Wang, X., Chen, X., Huang, W., Zhang, P., Guo, Y., Körner, H., Wu, H., Wei, W., 2019. Losartan suppresses the inflammatory response in collagen-induced arthritis by

inhibiting the MAPK and NF-κB pathways in B and T cells. Inflammopharmacology 27, 487–502.
Won, J.H., Park, S., Hong, S., Son, S., Yu, J.W., 2015. Rotenone-induced impairment of mitochondrial electron transport chain confers a selective priming signal for NLRP3 inflammasome activation. J. Biol. Chem. 290, 27425–27437.
Yang, S., Yao, B., Zhou, Y., Yin, H., Zhang, M.Z., Harris, R.C., 2012. Intrarenal dopamine modulates progressive angiotensin II-mediated renal injury. Am. J. Physiol. Ren. Physiol. 302, F742–F749.
Zeng, J., Wang, X., Pan, F., Mao, Z., 2022. The relationship between Parkinson's disease and gastrointestinal diseases. Front. Aging Neurosci. 14, 955919.
Zhang, C., Yang, Y., 2023. Targeting toll-like receptor 4 (TLR4) and the NLRP3 inflammasome: novel and emerging therapeutic targets for hyperuricaemia nephropathy. Biomol Biomed 24, 688–697.